Structures 5 (2016) 58–66

Contents lists available at ScienceDirect

Structures

journal homepage: http://www.elsevier.com/locate/structures

Concrete filled elliptical steel tubular members with large diameter-to-thickness ratio subjected to bending

Kojiro Uenaka [a,*], Hisao Tsunokake [b]

[a] Department of Civil Engineering, Kobe City College of Technology, Gakuenhigashimachi 8-3, Nishi, Kobe 6512194, Japan
[b] Department of Urban Engineering, Osaka City University, Sugimoto 3-3-138, Sumiyoshi, Osaka 5588585, Japan

ARTICLE INFO

Article history:
Received 23 February 2015
Received in revised form 24 July 2015
Accepted 17 August 2015
Available online 1 September 2015

Keywords:
Concrete filled elliptical steel tubular member
Symmetric four-point loading test
Diameter-to-thickness ratio
Pure bending capacity
Confinement effect

ABSTRACT

Concrete filled elliptical steel tubes, hereafter called CFESTs, are elliptical steel tube members filled in with concrete. The CFEST belongs to a family of concrete filled steel tubes, the so-called CFT, having good deformability and large seismic strength due to confined effect between the tube and in-filled concrete. The present study aims to investigate experimentally the characteristics of the CFEST members under pure bending. The selected testing parameters are diameter-to-thickness ratio of elliptical steel tube and loading directions, namely, the minor and major axes directions. From the test results, both local buckling and cracking of the steel tube can be observed in compressive and tensile regions, respectively. Obtained pure bending strength of the CFEST is strongly affected by diameter-to-thickness ratio. Pure bending capacity of the CFEST is also compared to that of the circular CFT. Methods to predict pure bending strength of the CFEST based on concrete strength, yielding and fracture points of the steel tube and confinement effect are described. Moreover, pure bending strength of the CFEST members is mainly discussed in comparison to that of ordinary CFT members. Additionally, biaxial stress behavior of the steel tube induced by in-filled concrete is also mentioned.

1. Introduction

Concrete filled elliptical steel tubes, hereafter called CFEST, consist of elliptical steel tube members filled in with concrete as shown in Fig. 1. CFEST members belong to the concrete filled steel tube, CFT [1,2] family, holding good deformability and large seismic strength. When a CFEST member is applied to a steel–concrete composite bridge pier located at a river, reduction of the bottom scouring due to the water flow can be expected.

Reviewing the past studies on elliptical hollow sections, EHS or CFEST (in-filled EHS), we can first find that elliptical steel tube and in-filled or un-filled concrete stub column tests [3,4,5]. Second, minor and major axes bending-shear tests of EHS beam were performed by Chan [6] and Gardner [7]. Then, flexural behavior of stainless steel oval hollow section (OHS) was investigated by Theofanous et al. [8]. Third, elastic buckling behavior and cross-section classification of EHS/OHS were discussed by Ruiz-Teran and Gardner [9] and Gardner and Chan [10]. Willibald et al. [11] and Sauced [12] investigated new applications of the EHS gusset plate connections which are regularly used in steel frames. Next, Episons et al. [13] conducted analytical studies on the fire resistance behavior of concrete filled EHS under compression. Last, studies on concrete filled EHS stub columns under eccentric compression were carried out experimentally by Sheehan et al. [14], and Insausti [15] carried out numerical studies applying a model of plastic collapse of EHS.

Under the above-described background, the authors have conducted 21 axially loading tests on CFEST stub columns with large diameter-to-thickness ratio ($2a/t$) and aspect ratios (a/b), which ranged from 69.6 to 160.0 and 1.5 to 2.5, respectively [16]. From the results of the stub column tests, it can be found that confinement effect between in-filled concrete and steel tubes did not change when diameter-to-thickness ratio ($2a/t$) became larger. In order to apply CFEST in practical use, it is necessary to investigate the mechanical behavior of CFEST members.

The present study aims to investigate experimentally the pure bending characteristics of the CFEST beams with large diameter-to-thickness ratio ($2a/t$) ranging from 69.6 to 160.0 through the symmetric four-point loading testing method. Two testing parameters were selected: diameter-to-thickness ratio of elliptical steel tubes and loading directions, namely, minor and major axes. Moreover, pure bending behavior of CFEST member is compared with that of an ordinary CFT member, whose diameter-to-thickness ratio ($2a/t$) ranges from 34.8 to 160.0. A method to predict the pure bending capacity of CFEST beam is mainly discussed and biaxial stress behavior of the elliptical steel tubes is provided. A part of this study has been previously reported [17,18].

2. Experimental testing

2.1. Test specimens

Figs. 2 and 3 and Table 1 show the details of the test specimens. The length (larger diameter) and aspect ratio of elliptical steel tubes were

* Corresponding author.

http://dx.doi.org/10.1016/j.istruc.2015.08.004
2352-0124/

Nomenclature

a and b	larger and smaller radii of the elliptical steel tubes
t	tube's thickness of elliptical steel section
f_c'	concrete strength
f_y	yielding point of the steel tube
f_u	fracture point of the steel tube
ν	Poisson's ratio of steel tube
M	applied bending moment
ϕ	curvature of CFEST
M_{exp}	experimental bending strength
M_{est}	estimation of ultimate bending moment based upon yielding point
N_{est}	estimation of ultimate axial load based upon yielding point
$M_{est\text{-}u}$	estimation of ultimate bending moment based upon fracture point
$N_{est\text{-}u}$	estimation of ultimate axial load based upon fracture point
α	angle between bottom of compressive area and neutral axis
$M_{est\text{-}aij}$	estimated bending strength based on CFT in AIJ
$N_{est\text{-}aij}$	estimated axial force based on CFT in AIJ
$_c\sigma_{cB}$	concrete strength induced by confined effect
σ_r	confined stress induced by external tube proposed by AIJ
ε_z and ε_θ	axial and circumferential strains of the tube
σ_z and σ_θ	axial and circumferential stresses of the tube

160 mm and 2.0, respectively. Concrete filled circular steel tubes (CFT) having diameters of 80 mm and 160 mm were prepared to be compared with the CFEST members. The thicknesses of the elliptical/circular steel tubes were 1.0, 1.6 and 2.3 mm. Thus, the larger diameter-to-thickness ratio ($2a/t$) ranged from 66.9 to 160.0. Elliptical/circular tubes having two welded plates at both ends were connected to rigid lateral beams through ten high-tension bolts.

Fig. 4 illustrates the testing apparatus. Pure bending moment ($M = Pl_1/2$, where P: Applied load) without shear force was applied to the specimens through the symmetric four-point loading testing method using the 500 kN universal testing machine located at Kobe City College of Technology(KCCT) as shown in Fig. 5.

2.2. Measurements

Fig. 2 shows the arrangement of the strain gages. Four biaxial strain gages were attached on the external surface of the steel tube to obtain

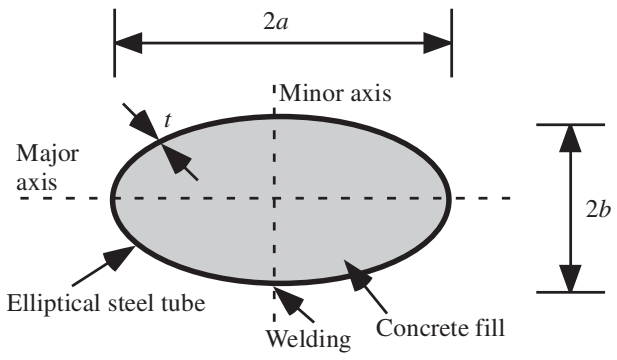

Fig. 1. Cross sectional area of the CFEST.

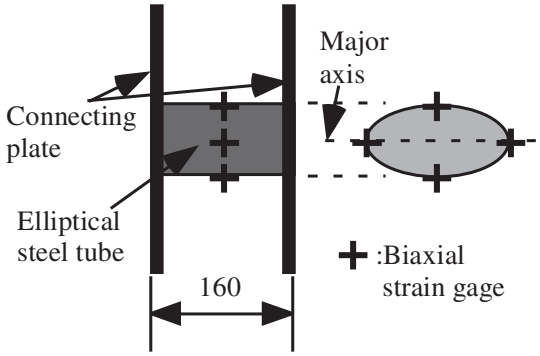

Fig. 2. Detail of the specimens and position of strain gages (minor axis test).

stress condition of elliptical and circular steel tubes. Three displacement transducers were placed under the specimens to obtain bending deformabilities of the CFEST beam as illustrated in Fig. 4. The experimental test was terminated when the fatal failure of the specimen was observed.

3. Results and discussion

3.1. Failure modes

Observed failure modes are shown in Fig. 6. Fig. 6(a) and (b) shows the ultimate states of the CFEST specimens after major and minor axes tests, respectively. In all the specimens, tensile failure in the tensile region occurred after local buckling of the tubes in the compressive region. No effect of diameter-to-thickness ratio ($2a/t$) on the failure modes could be found. Furthermore, Fig. 6(c) and (d) shows failure modes of CFT specimens with $D = 80$ and 160 mm. Failure modes of the CFEST member coincided with those of the CFT. No cracking of welding of two connecting plates can be found. Therefore, pure bending moment can be correctly applied to the specimens.

3.2. Bending deformability

The applied bending moment (M) plotted against central displacement is shown in Fig. 7, where panels (a) and (c) are the CFEST and panels (b) and (d) are the CFT specimens, respectively. In all test results, bending deformability increased as the larger diameter-to-thickness ratio ($2a/t$) decreased. Furthermore, displacement of CFT specimen having $D = 160$ mm with $t = 1.6$ and 1.0 mm decreased drastically to

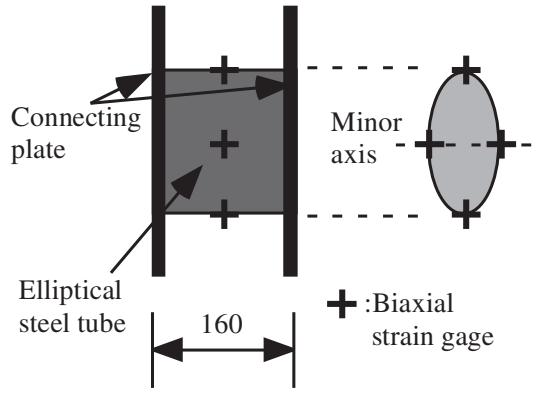

Fig. 3. Detail of the specimens and position of stain gages (major axis test).

Table 1
List of the specimens.

No.	Tag	Elliptical steel tube									Concrete
		Thick.	Diameter		Ratio		Length	Axis	f_y	f_u	f_c'
		t (mm)	$2a$ (mm)	$2b$ (mm)	$2a/t$	$2b/t$	L (mm)		(N/mm^2)	(N/mm^2)	(N/mm^2)
1	10-major	1.0	160	80	160.0	80.0	160	Major	196.0	345.4	37.9
2	10-minor	1.0	160	80	160.0	80.0		Minor			
3	16-major	1.6	160	80	100.0	50.0		Major	313.3	358.0	
4	16-minor	1.6	160	80	100.0	50.0		Minor			
5	23-major	2.3	160	80	69.6	34.8		Major	298.7	373.4	
6	23-minor	2.3	160	80	69.6	34.8		Minor			
7	10-c-80	1.0	80		80.0			–	196.0	345.4	36.8
8	10-c-160	1.0	160		160.0						
9	16-c-80	1.6	80		50.0				313.3	358.0	
10	16-c-160	1.6	160		100.0						
11	23-c-80	2.3	80		34.8				298.7	373.4	
12	23-c-160	2.3	160		69.6						

22 mm. The major, minor and CFT with $D = 80$ mm specimens regulated maximum bending moment for displacements over the 30 mm.

Fig. 8(a) gives the relationship between applied bending moment (M) and curvature(ϕ). The curvature is approximately calculated applying the three displacement transducers as shown in Fig. 8(b), in which δ is the difference between central and average of two sides' displacements. In addition, curvature obtained from axial strain distribution is shown in Fig. 8(c). All the specimens having curvature values within $\phi = 0.1$ (1/m) reached their maximum values. Pure bending strengths of CFEST and CFT members were almost kept from 0.1 to 0.3 (1/m). Bending moment maintains maximum value over the curvature being 0.2(1/m).

Last, the specimen 23-c-160 showed the difference behavior of two curvatures. Very little different displacement was recorded by three displacement transducers at an initial loading owing to the largest bending stiffness and the length equivalent to the diameter of the specimen.

3.3. Bending strength

3.3.1. Effect of diameter-to-thickness ratio

Fig. 9 gives the relationship between larger diameter-to-thickness ratio, $2a/t$ and ultimate bending capacity (M_{exp}). The bending capacity decreased as larger diameter-to-thickness ($2a/t$) ratio increased. This is because the cross section of steel tube decreased as diameter-to-thickness ratio increased. This phenomenon coincided with that of pure bending characteristics of CFT.

3.3.2. Predicted strength

Concrete filled elliptical steel tube stress distribution at ultimate state can be assumed as illustrated in Fig. 10, where Fig. 10(a) and (b) are the major and minor axis tests, respectively. For example, the ultimate

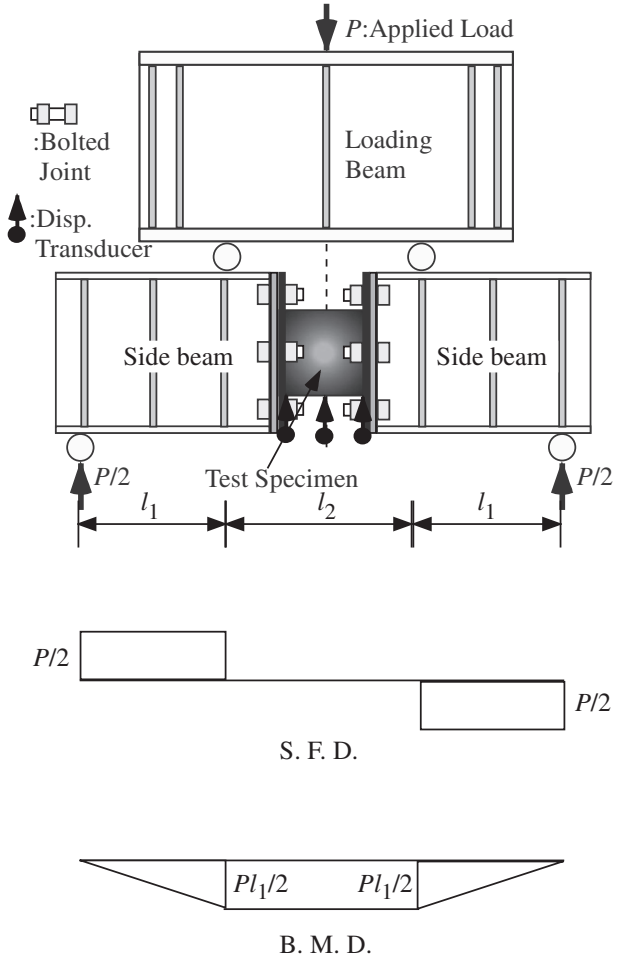

Fig. 4. Loading method.

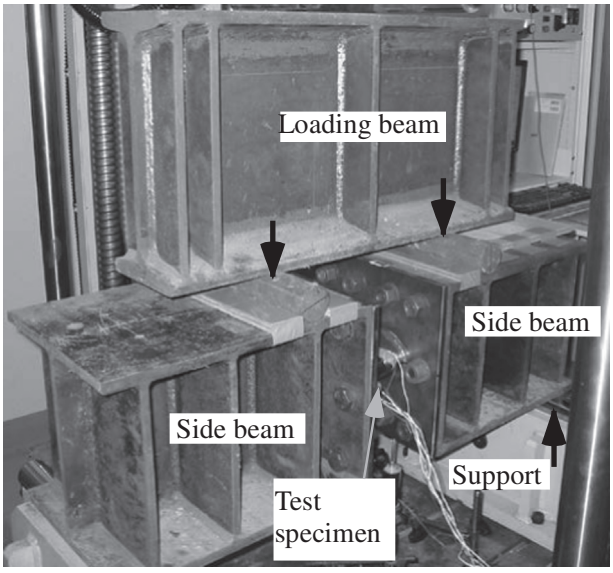

Fig. 5. Test apparatus.

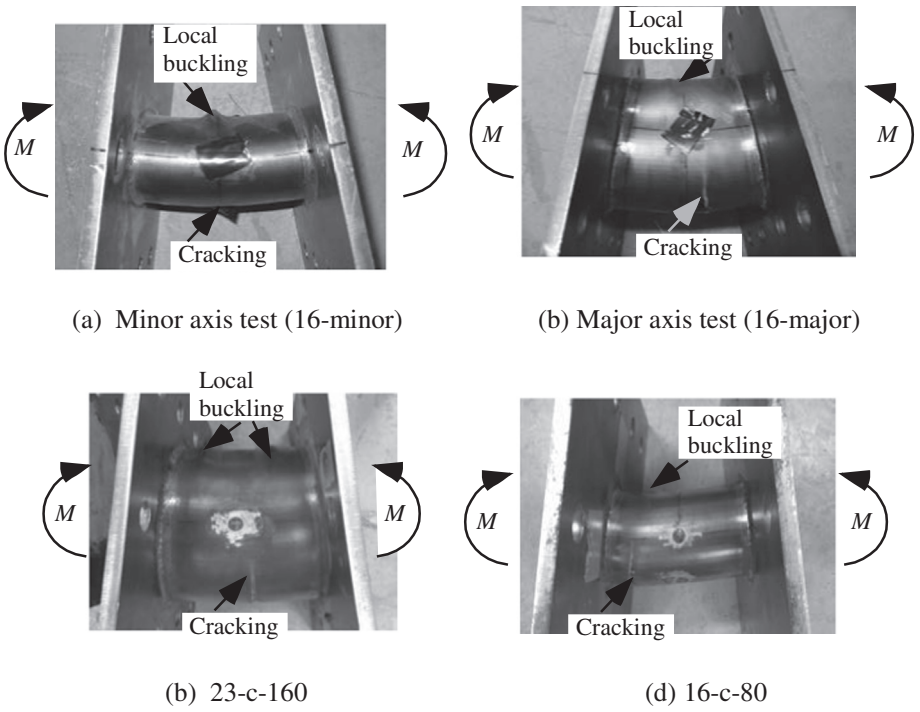

Fig. 6. Failure modes.

bending moment (M_{est}) and axial force (N_{est}) at ultimate state of the minor axis test, in the same methods of the CFT [2,19] subjected to simultaneous bending moment and axial load, can be expressed as below,

$$M_{est} = \frac{2}{3}kf'_c(a-t)(b-t)^2\cos^3\alpha + \frac{4}{3}f_y\left\{ab^2-(a-t)(b-t)^2\right\}\cos^3\alpha \quad (1)$$

$$N_{est} = \frac{kf'_c}{2}(a-t)(b-t)(\pi-2\alpha-\sin 2\alpha) - f_y t(a+b-t)(\sin 2\alpha + 2\alpha) \quad (2)$$

where k: reduction factor of concrete (=0.85); a and b: larger and smaller radii of the elliptical steel tubes; t: thickness of the steel tube; and α: angle between bottom of compressive area and neutral axis.

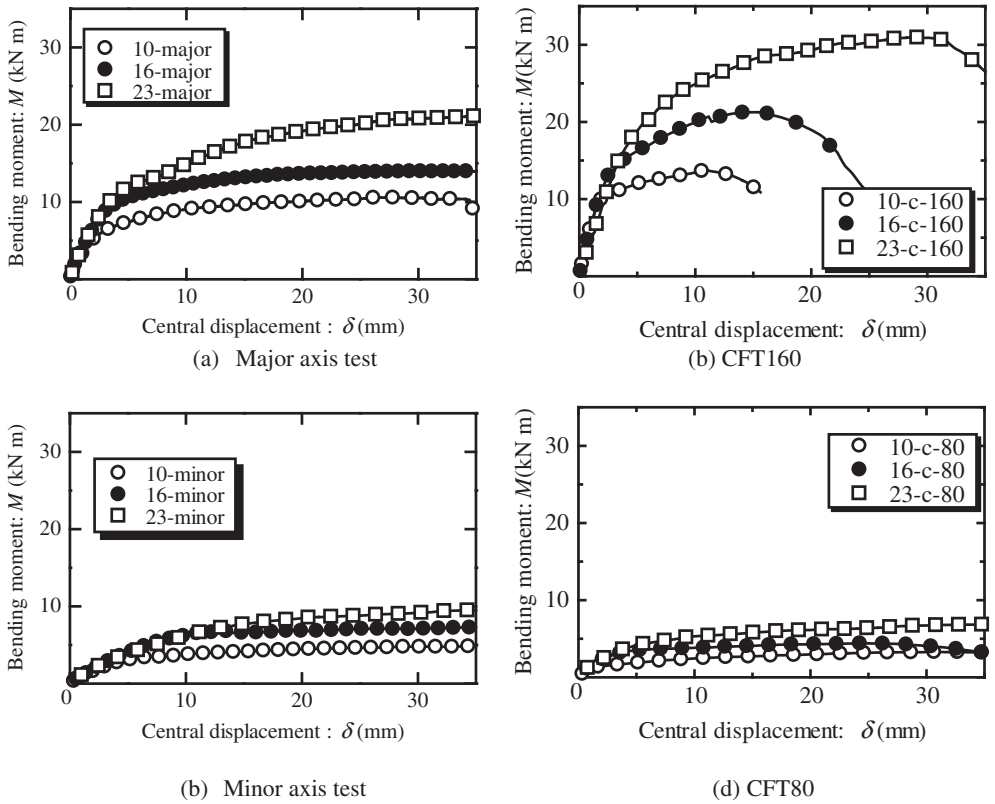

Fig. 7. Bending moment and displacement.

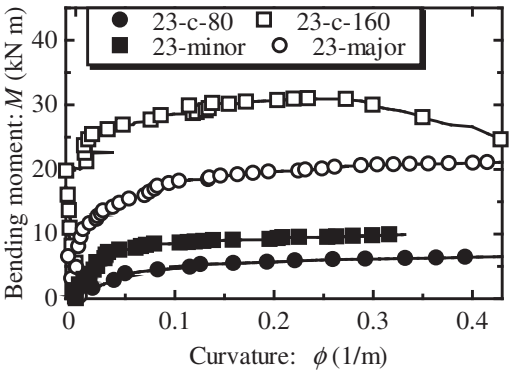

(a) Curvature calculated by displacement

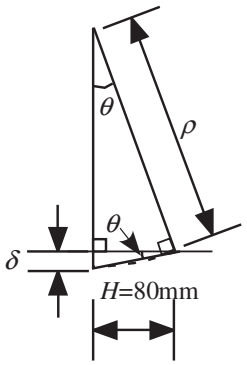

(b) Calculate method

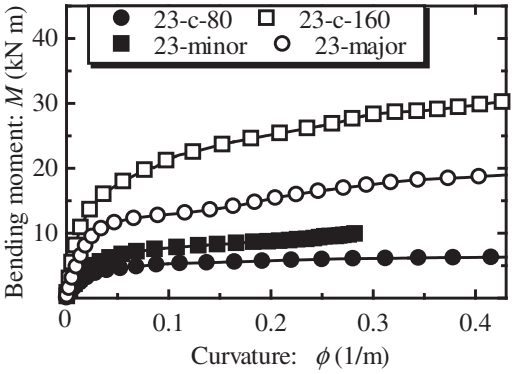

(c) Curvature calculated by strain distribution

Fig. 8. Curvature.

According to axial and bending strengths of the CFT member [2], axial strength ($N_{est\text{-}aij}$) and bending moment ($M_{est\text{-}aij}$) of the minor axis test of the CFEST can be calculated as below,

$$M_{est-aij} = \frac{2}{3}{}_c\sigma^c{}_{cB}(a-t)(b-t)^2\cos^3\alpha + \frac{2}{3}f_y\left\{ab^2-(a-t)(b-t)^2\right\} \times(\beta_1+\beta_2)\cos^3\alpha \quad (3)$$

$$N_{est-aij} = \frac{{}_c\sigma^c{}_{cB}}{2}(a-t)(b-t)(\pi-2\alpha-\sin2\alpha)+\frac{f_y}{2}t(a+b-t) \times\{\pi(\beta_1-\beta_2)-(\beta_1+\beta_2)(\sin2\alpha+2\alpha)\} \quad (4)$$

where, β_1 and β_2: confinement factors which are 0.89 and 1.08, respectively, as specified in AIJ [1]. To estimate the major axis test results, $a(b)$ is replaced by $b(a)$ in Eqs. (1) to (4),

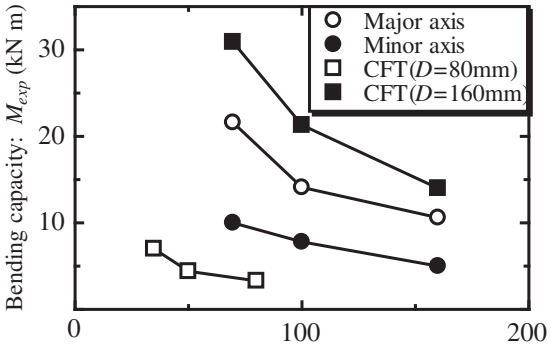

Fig. 9. Larger diameter-to-thickness ratio and bending capacity.

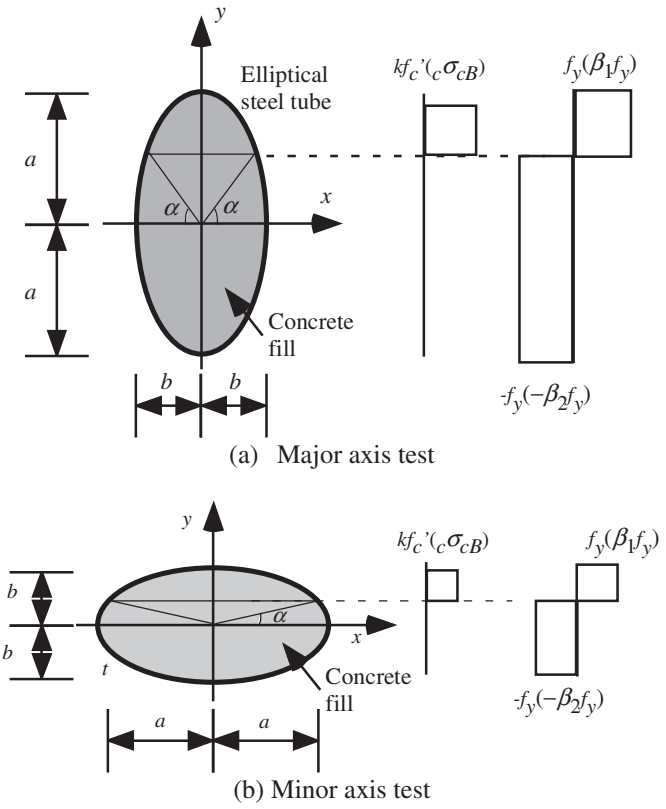

Fig. 10. Assumption of stress distribution at ultimate state.

Table 2
Testing results and estimations.

No.	Tag	P_u	[1] M_{exp}	[2] M_{est}	[3] M_{est_u}	[4] M_{est_aij}	[5] M_{est_aiju}	[1]/[2]	[1]/[3]	[1]/[4]	[1]/[5]
		(kN)	(kN m)	(kN m)	(kN m)	(kN m)	(kN m)				
1	10-major	81.0	10.6	4.8	7.9	5.2	8.6	2.21	1.34	2.05	1.23
2	10-minor	38.5	5.0	2.6	4.5	2.8	4.7	1.95	1.13	1.82	1.07
3	16-major	108.0	14.1	10.9	12.2	11.9	13.4	1.30	1.16	1.19	1.06
4	16-minor	59.8	7.8	6.2	7.0	6.7	7.5	1.26	1.11	1.18	1.04
5	23-major	164.6	21.6	14.1	17.2	15.6	19.0	1.52	1.25	1.39	1.13
6	23-minor	76.6	10.0	8.2	10.1	8.8	10.8	1.23	0.99	1.14	0.93
7	10-c-80	25.1	3.3	1.6	2.7	1.7	2.9	2.04	1.21	1.90	1.13
8	10-c-160	106.8	14.0	6.8	11.6	7.4	12.5	2.06	1.21	1.89	1.12
9	16-c-80	33.6	4.4	3.7	4.2	4.0	4.5	1.18	1.05	1.09	0.97
10	16-c-160	162.4	21.3	16.2	18.4	17.5	19.7	1.31	1.16	1.22	1.08
11	23-c-80	53.6	7.0	4.8	5.9	5.2	6.4	1.46	1.19	1.34	1.09
12	23-c-160	236.2	30.9	21.4	26.2	23.1	28.1	1.45	1.18	1.34	1.10
Mean								1.58	1.16	1.46	1.08
Coefficient of variation (COV)								0.23	0.07	0.23	0.07

In-filled concrete strength ${}_c\sigma_{cB}$ being induced by confinement effect of circular steel tube can be calculated as below [2],

$${}_c\sigma^c{}_{cB} = f'_c + k \cdot \sigma_r \tag{5}$$

where k: coefficient of confinement effect ($=4.1$); σ_r: confined stress induced by external tube proposed by AIJ [2] can be expressed as below,

$$\sigma_r = 0.19\frac{t}{b-t}f_y \tag{6}$$

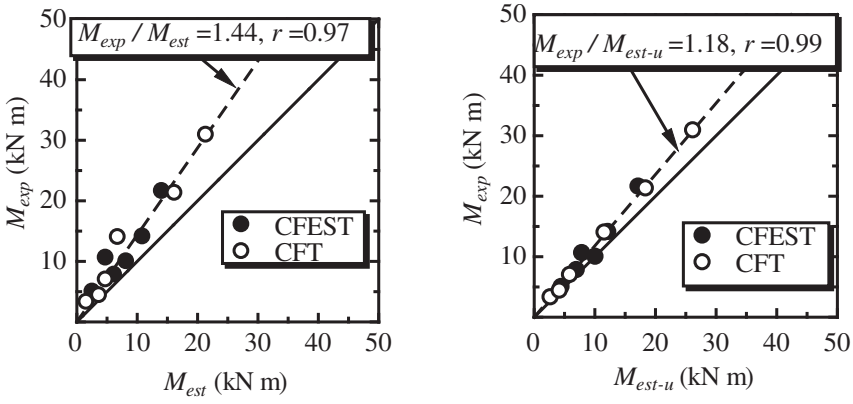

(a) M_{est} based upon f_y (b) M_{est-u} based upon f_u

Fig. 11. Estimations and experiments.

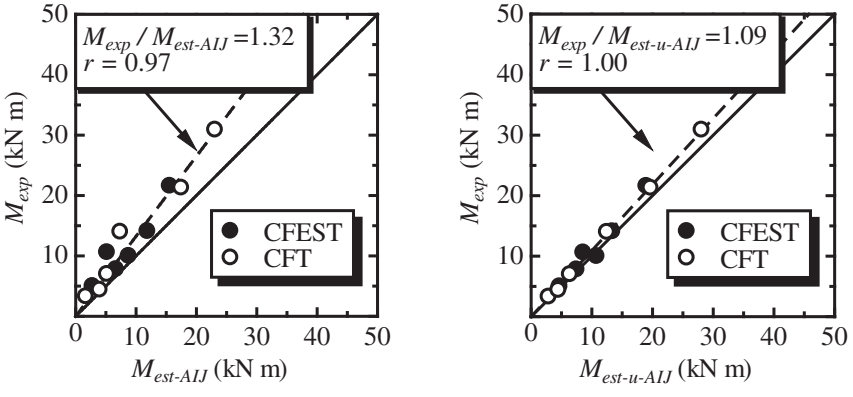

(a) $M_{est-AIJ}$ based upon f_y (b) $M_{est-u-AIJ}$ based upon f_u

Fig. 12. Estimations induced by confinement effect and experiments.

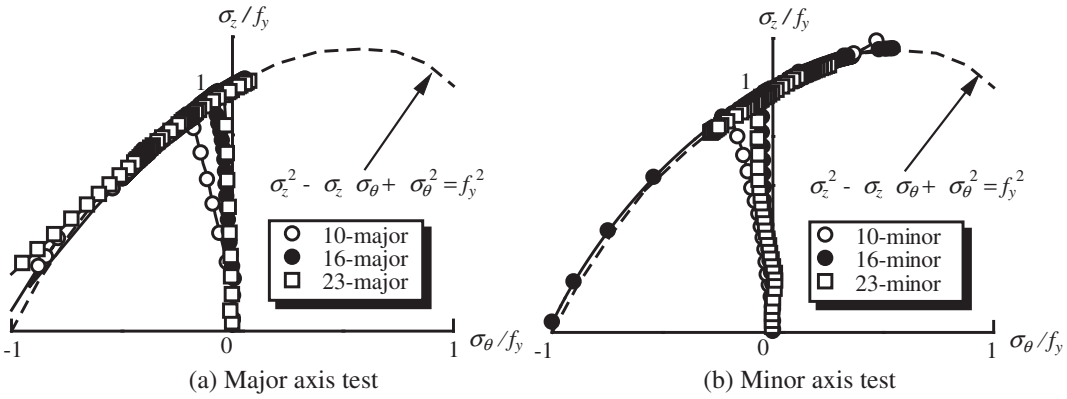

Fig. 13. Biaxial stress condition of CFEST (compressive region under bending).

where b is the smaller radius of the tube.

Estimated pure bending moments can be obtained according to the following steps. First, the degree α_0, for axial force equal to zero, can be calculated from Eq. (2). Then introducing α_0 into Eq. (1), pure bending moment (M_{est}) can be obtained. The calculated strengths are summarized in Table 2.

Fig. 11(a) shows the relationship between the experimental results (M_{exp}) and estimative results (M_{est}) for all specimens. All the specimens are larger than the estimative results as shown in Fig. 11(a), and strength ratio (M_{exp}/M_{est}) and correlation factor (r) are 1.44 and 0.97, respectively. Furthermore, Fig. 11(b) shows the relationship between experimental results (M_{exp}) and the estimative results ($M_{est\text{-}u}$) based upon the fracture strength f_u obtained by coupon tensile test, instead of f_y of Eqs. (1) and (2). The experimental results (M_{exp}) are in good agreement with the estimations ($M_{est\text{-}u}$) rather than the values of M_{est} obtained based upon f_y, namely, $M_{exp}/M_{est\text{-}u}$ ratio and correlation factor(r) of 1.18 and 0.99, and the calculated value ($M_{est\text{-}u}$) underestimates the ultimate strength up to 32%. This is due to the strain hardening of steel tubes, that is, the tensile strain was recorded over 10%.

Fig. 12(a) and (b) shows the relationship between estimated bending moment M_{exp} and $M_{est\text{-}AIJ}$ calculated by Eqs. (3) and (4). In Fig. 12(a), experimental bending moment, M_{exp} is also larger than the estimations, $M_{est\text{-}AIJ}$. Furthermore, experimental strength M_{exp} coincided with $M_{est\text{-}u\text{-}AIJ}$ calculated by Eqs. (3) and (4), in which f_y was replaced by f_u as shown in Fig. 12(b). This fact indicates that the pure bending strength of the CFEST member can be correctly predicted by adopting confined concrete strength and ultimate steel strength, namely, difference between $M_{est\text{-}u\text{-}AIJ}$ and M_{exp} is up to 23%.

Lastly, the axial force may be induced by two side beams owing to small 160 mm in length of the specimens in this study. Therefore, we recommend estimating pure bending strength by Eqs. (1) and (2). Additionally, in the specimen with larger than 160 mm in length, experimental strength might be larger than the estimations.

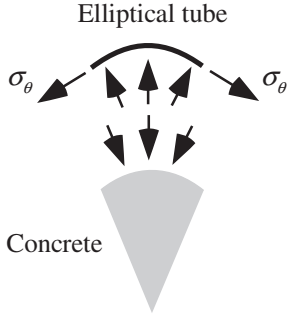

Fig. 14. Stress condition between the tube and concrete under bending-compression.

3.4. Biaxial stress condition

3.4.1. Calculation of elasto-plastic stress

Four strain gages were attached to record biaxial strain behavior of the elliptical steel tubes. According to von Mises design criteria, yielding stress under plane stress condition can be expressed as below,

$$f_s = \sigma_z^2 - \sigma_z \cdot \sigma_\theta + \sigma_\theta^2 - f_y^2 \tag{5}$$

where σ_z and σ_θ are the axial and circumferential stresses of the steel tube. When the two stresses are within the elastic range, that is, $f_s < 0$, their stresses can be calculated as below,

$$\begin{Bmatrix} d\sigma_z \\ d\sigma_\theta \end{Bmatrix} = \frac{E}{1-\nu^2}\begin{bmatrix} 1 & \nu \\ \nu & 1 \end{bmatrix}\begin{Bmatrix} d\varepsilon_z \\ d\varepsilon_\theta \end{Bmatrix}. \tag{6}$$

where ε_z and ε_θ are the axial and circumferential strains, respectively.

When the two stresses enter the plastic range, that is, $f_s = 0$, elasto-plastic stress can be calculated as below,

$$\begin{Bmatrix} d\sigma_z \\ d\sigma_\theta \end{Bmatrix} = \left\{\frac{E}{1-\nu^2}\begin{bmatrix} 1 & \nu \\ \nu & 1 \end{bmatrix} - \frac{1}{S}\begin{bmatrix} S_1^2 & S_1S_2 \\ S_1S_2 & S_2^2 \end{bmatrix}\right\}\begin{Bmatrix} d\varepsilon_z \\ d\varepsilon_\theta \end{Bmatrix} \tag{7}$$

where E and ν are the Young's modulus and Poisson ratio of steel tubes, respectively. S, S_1 and S_2 can be obtained as below,

$$S = s_z S_1 + s_\theta S_2, S_1 = \frac{E}{1-\nu^2}(s_z + \nu s_\theta), S_2 = \frac{E}{1-\nu^2}(s_\theta + \nu s_z). \quad (8\text{ a, b, c})$$

where s_z and s_θ are the deviatoric stresses in the axial and circumferential directions, respectively. Compressive stress and strain are considered as positive.

The two elasto-plastic stresses can be obtained as below,

$$\sigma_z = \sum d\sigma_z, \sigma_\theta = \sum d\sigma_\theta. \tag{9 a, 9b}$$

3.4.2. Biaxial stress conditions under bending-compression

The relationship between axial and circumferential stresses (σ_z and σ_θ) of elliptical steel tubes in the compressive region is given in Fig. 13(a) and (b). x and y axes are normalized by the yielding points of steel tubes. When the two stresses reached yielding surface, they flowed towards the tensile-compressive region in the major axis test as shown in Fig. 13(b). This is due to the volumetric dilatation of the concrete in-fill as shown in Fig. 14. On the other hand, circumferential stress of minor axis test remained in compressive region as shown in Fig. 13(b). This may be due to the smaller influence of volumetric dilatation than in the case of the major axis test in compressive region.

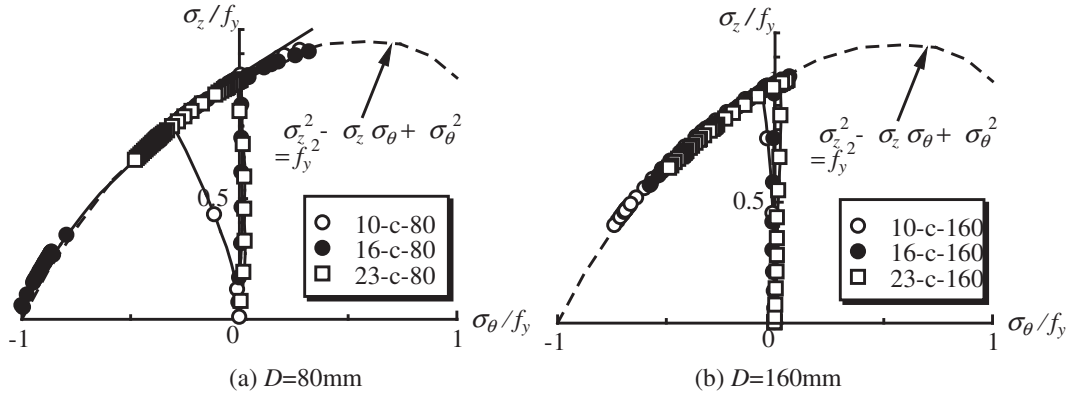

Fig. 15. Biaxial stress condition of CFT (compressive region under bending).

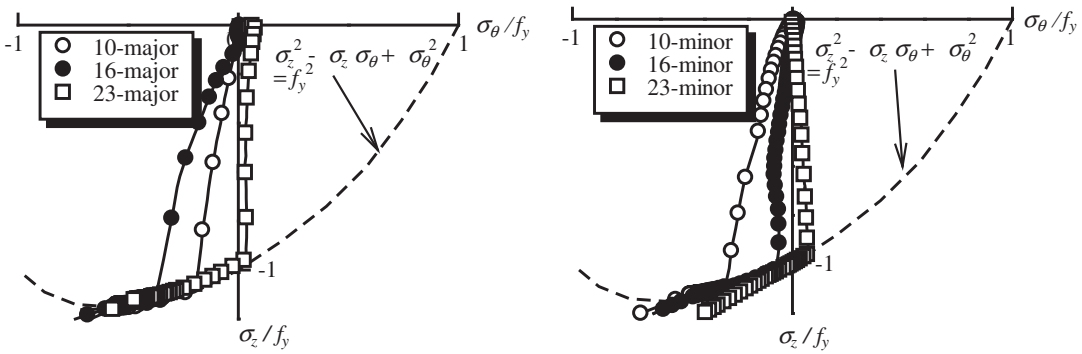

Fig. 16. Biaxial stress condition of CFEST (neutral axis).

Fig. 15(a) and (b) provides biaxial stress conditions of the CFT specimens under bending-compression. The circumferential stress (σ_θ) flowed towards the tensile region after the two stresses reached yielding surface. This fact can be explained in terms of volumetric dilatation of the finding in Fig. 13(a). The biaxial behavior of the CFEST beam under bending-compression coincided with that of the CFT.

3.4.3. Biaxial stress conditions under bending-tension

Fig. 16(a) and (b) provides the relationship between axial and circumferential stresses of elliptical steel tubes at the central axis. The axes of the diagram are also normalized by the yielding point, f_y. No axial compressive stress could be found, in other words, the neutral axis shifted to the compressive region after cracking. Both axial and circumferential stresses (σ_z and σ_θ) flowed towards tensile–tensile region after attaining to yielding surface. This phenomena can suggest that the confined stress exists in the filled concrete as shown in Fig. 17.

Biaxial stress histories of the CFT in tensile region are also shown in Fig. 18(a) and (b). The two biaxial stresses flowed towards tensile–tensile region. This fact is explained in terms of the confinement by cracking of the concrete in-fill as described in the stress behavior of the elliptical steel tubes. The biaxial stress behavior of the CFEST beam under bending-tension coincided with that of the CFT again.

4. Conclusions

Concrete filled elliptical steel tubular (CFEST) members with large diameter-to-thickness ratio subjected to pure bending moment have been examined. Additionally, pure bending characteristics of the CFEST beams have been compared with that of ordinary CFT members. Considering two main testing parameters, diameter-to-thickness and two pure bending loading directions, namely, major and minor axes directions, the following conclusions can be drawn.

(1) Observed failure modes were both local buckling in compressive region and fracture in tensile region of elliptical steel tubes. These phenomena agreed with the results for ordinary CFT member under pure bending.
(2) Bending moment deformability increased as diameter-to-thickness ratio ($2a/t$) decreased. Moreover, the smallest deformability was found in the CFT specimens with D = 160 mm, which are the smallest diameter.
(3) Ultimate bending capacities (M_{exp}) of major, minor axis test specimens and CFT member with D = 80 mm were maintained for central displacement that were over 20 mm.

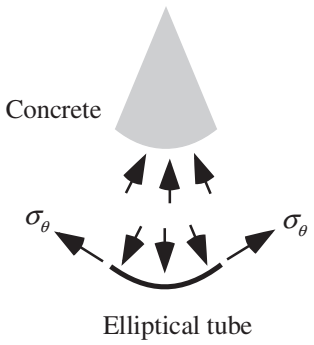

Fig. 17. Stress conditions between the tubes and the concrete under bending-tensile.

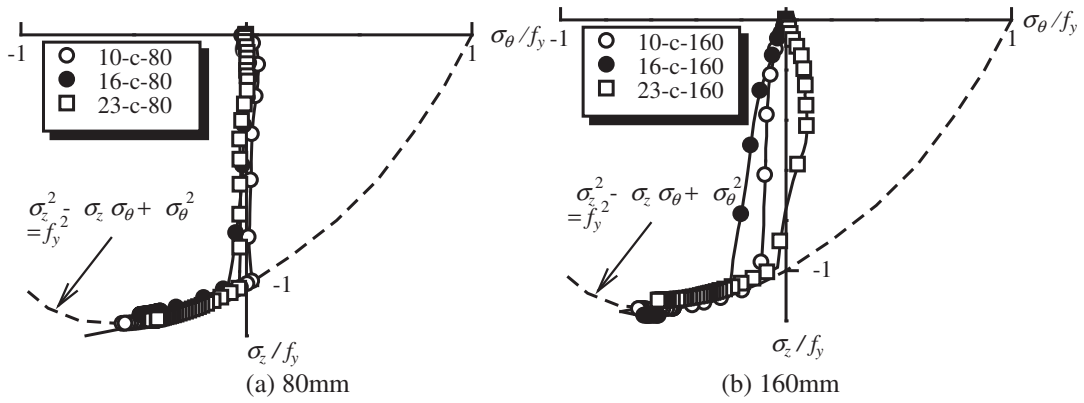

Fig. 18. Biaxial stress condition of CFT (neutral axis).

(4) Obtained bending capacities (M_{exp}) decreased as the larger diameter-to-thickness ratio ($2a/t$) increased. This is due to the reduction of confined stress induced by the steel tube.
(5) Bending capacities (M_{exp}) of the CFEST members were either in good agreement with, or larger than the estimations (M_{est} and $M_{est\text{-}u}$) based on bending strength. Furthermore, the bending capacities of the CFEST can be theoretically predicted by the Eqs. (3) and (4), where yielding point f_y is replaced with fracture point f_u.
(6) With respect to the CFT and major axis test specimens, circumferential stress (σ_θ) flowed towards the tensile region of steel tubes under bending compression after the two stresses reached the yielding surface. This is due to the volumetric dilatation of infilled concrete. On the other hand, for the specimens of minor axis test, circumferential stress (σ_θ) under bending compression remained independent of the volumetric dilatation.
(7) Circumferential stress (σ_θ) flowed towards the tensile region located at neutral axis after tensile yielding of axial stress (σ_z). This is due to the confinement effect induced by cracking in-filled concrete.
(8) From the results of above (6) and (7), the stress behavior of the steel tubes both bending compression and bending tension coincided with that of CFT.

Acknowledgment

The authors thank Mr. Yamamoto, T., Mr. Shimizu, S. and Mr. Ando, S., students of the Advanced Course in Kobe City College of Technology (KCCT) for their assistance during the experiment. Moreover, we would appreciate Ms. Ichinose L. H., the group manager of Japan Industrial Testing Corporation, for correcting the draft in English of this manuscript.

References

[1] Architectural Institute of Japan. Standard for Structural Calculation of Steel Reinforced Concrete Structures. Maruzen; 2002 (in Japanese).
[2] Architectural Institute of Japan. Recommendations for Design and Construction of Concrete Filled Steel Tubular Structures; 2008(in Japanese).
[3] Yang H, Lam D, Gardner L. Testing and analysis of concrete-filled elliptical hollow section. Eng Struct 2008;30(12):3771–81.
[4] Chan TM, Gardner L. Compressive resistance of hot-rolled elliptical hollow sections. Eng Struct 2008;30(2):522–32.
[5] Zhao XL, Packer JA. Tests and design of concrete-filled elliptical hollow section stub columns. Thin-Walled Struct 2009;47(6–7):617–28.
[6] Gardner L, Chan TM, Wadee MA. Shear response of elliptical hollow sections. Struct Build 2008;161(SB6):301–8.
[7] Chan TM, Gardner L. Bending strength of hot-rolled elliptical hollow sections. J Constr Steel Res 2008;64:971–86.
[8] Theofanous M, Chan TM, Gardner L. Flexural behaviour of stainless steel oval hollow sections. Thin-Walled Struct 2009;47(6–7):776–87.
[9] Ruiz-Teran AM, Gardner L. Elastic buckling of elliptical tubes. Thin-Walled Struct 2008;46(11):1304–18.
[10] Gardner L, Chan TM. Cross-section classification of elliptical hollow sections. Steel Compos Struct Int J 2007;7(3):185–200.
[11] Willibald S, Packer JA, Martinez-Sauced G. Behaviour of gusset plate connections to ends of round and elliptical hollow structural section members. Can J Civ Eng 2006; 33:373–83.
[12] Saucedo GM, Packer JA, Zhao XL. Static design of elliptical hollow section end-connections. Struct Build 2008;161(SB2):103–13.
[13] Espinos A, Gardner L, Romero ML, Hospitaler A. Fire behaviour of concrete filled elliptical steel column. Thin-Walled Struct 2011;49(2):239–55.
[14] Sheehan A, Dai XH, Chan TM, Lam D. Structural response of concrete-filled elliptical steel hollow sections under eccentric compression. Eng Struct 2012;45:314–23.
[15] Insausti A, Gardner L. Analytical modeling of plastic collapse in compressed elliptical hollow sections. J Constr Steel Res 2011;67:678–89.
[16] Uenaka K. Experimental study on concrete filled elliptical/oval steel tubular stub columns under compression. Thin-Walled Struct 2014;78:131–7.
[17] Uenaka K, Tsunokake H. Experimental Study on Concrete Filled Elliptical Steel Tubular Members Under Bending. Proceeding of Japan Concrete Institute, 35; 2013. p. 1159–64 (in Japanese).
[18] Uenaka K, Tsunokake H. Pure Bending Characteristics of Concrete Filled Elliptical Steel Tubular Members. Proceedings of The 6th International Conference of Asian Concrete Federation; 2014. p. 1079–84.
[19] Eurocode4. Design of Composite Steel and Concrete Structures—Part 1.1: General Rules and Rules for Buildings, EN 1994-1-1; 2004.